

# On the X-ray and optical properties of the Be star HD 110432: a very hard-thermal X-ray emitter<sup>★</sup>

R. Lopes de Oliveira<sup>1,2</sup>, C. Motch<sup>2</sup>, M.A. Smith<sup>3</sup>, I. Negueruela<sup>4</sup>, and J.M. Torrejón<sup>4</sup>

<sup>1</sup> Instituto de Astronomia, Geofísica e Ciências Atmosféricas, Universidade de São Paulo, R. do Matão 1226, 05508-900 São Paulo, Brazil

<sup>2</sup> Observatoire Astronomique, UMR 7550 CNRS, 11 rue de l'Université, F-67000 Strasbourg, France

<sup>3</sup> Catholic University of America, 3700 San Martin Drive, Baltimore, MD 21218

<sup>4</sup> Departamento de Física, Ingeniería de Sistemas y Teoría de la Señal, Escuela Politécnica Superior, Universidad de Alicante, Ap. 99, 03080 Alicante, Spain

Received/Accepted - **draft**

**Abstract.** HD 110432 is the first proposed, and best studied, member of a growing group of Be stars with X-ray properties similar to  $\gamma$  Cas. These stars exhibit hard-thermal X-ray emissions that are variable on all measurable timescales. This emission contrasts with the soft emission of “normal” massive stars and with the nonthermal emission of all well known Be/X-ray binaries – so far, all Be + neutron star systems. In this work we present XMM-*Newton* X-ray spectra and light curves in addition to new optical spectroscopic and photometric observations. Like  $\gamma$  Cas, the X-rays of HD 110432 appear to have a thermal origin, as supported by strongly ionized Fe XXV and Fe XXVI lines detected in emission. A fluorescent iron feature at 6.4 keV is present in all observations, while the Fe XXVI Ly $\beta$  line is present in two of them. Its X-ray spectrum, complex and timing dependent, is well described in each observation by three thermal plasmas with temperatures ranging between 0.4–0.7, 3–6, and 21–37 keV, as *cool*, *warm*, and *hot* components, respectively. Thus, HD 110432 has the hottest thermal plasma of any known Be star. A sub-solar iron abundance ( $\sim 0.3\text{--}0.5 \times Z_{Fe,\odot}$ ) is derived for the hottest plasma, while lines of less excited ions at longer wavelengths are consistent with solar abundances. The star has a moderate 0.2–12 keV luminosity of  $\sim 5 \times 10^{32}$  erg s $^{-1}$ . The intensity of the X-ray emission is strongly variable. Recurrent flare-like events on time scales as short as  $\sim 10$  seconds are superimposed over a slowly  $\sim 5\text{--}10 \times 10^3$  seconds varying basal flux, followed by similarly rapid hardness variabilities. There is no evidence for short pulsations from 0.005 to 2.5 Hz, and an upper limit of  $\sim 2.5\%$  is derived on the pulsed fraction. Except for a  $\sim 14000$  seconds oscillation recurrent in the hardness for two of the three XMM-*Newton* observations, no periodicity is detected in low frequencies. In the optical region the strong and quasi-symmetrical profile of the H $\alpha$  line (EW  $\sim -60$  Å) as well as the detection of several metallic lines in emission strongly suggest a dense and/or large circumstellar disk. Also, the double-peaked profiles of metallic lines confirm the nearly edge-on projection of that disk noted recently by Smith & Balona. HD 110432 has several properties reminiscence of the cataclysmic variables such as a very hot X-ray temperature and its detailed spectral features. This suggests that it might be a Be star harbouring an accreting white dwarf. On the other hand, accumulating evidence of magnetic activities in the literature supports the surface-disk of the star as being the X-ray site.

**Key words.** stars: emission-line, Be – stars: individual: HD 110432.

## 1. Introduction

Although  $\gamma$  Cas (B0.5 Ve) has long stood out as having unique X-ray properties among massive stars, accumulating evidence suggests that it is only the first of a growing subclass of X-ray active Be stars. HD 110432

(B1IVe; Smith & Balona 2006) was the first proposed  $\gamma$  Cas analog on the basis of its mean 2–10 keV fluxes and energy distribution, and optical and X-ray variability properties (Robinson et al. 2002; Smith & Balona 2006). Other similar objects are HD 161103, SAO 49725, USNO 0750–13549725, SS 397 (Motch et al. 1997, 2006; Lopes de Oliveira et al. 2006), and HD 119682 (Rakowski et al. 2006; Safi-Harb et al. 2006). Altogether, these objects point to a new class of X-ray emitters (Motch et al. 2006; Lopes de Oliveira et al. 2006) composed of Be stars having an unusual hard-thermal X-ray emission ( $kT \gtrsim 7$  keV)

Send offprint requests to: R. Lopes de Oliveira,  
e-mail: rlopes@astro.iag.usp.br

<sup>★</sup> Based on observations obtained with XMM-*Newton*, an ESA science mission with instruments and contributions directly funded by ESA Member States and NASA.

of moderate luminosity (few  $10^{32}$  erg s $^{-1}$ , at 0.2–12 keV), which displays marked variability on long and short time scales. However, in contrast with the behaviour of many Be/X-ray systems, no outburst has yet been observed from any  $\gamma$  Cas system. Curiously, all known members are B0.5–1 stars.

The nature of the X-ray emission of  $\gamma$  Cas and its analogs is currently a matter of controversy. Two exciting interpretations have been proposed in the recent literature: [1] single-Be stars with unusually strong magnetic activity, and tentatively associated to progenitors of magnetars, [2] binary systems with an accreting degenerate companion – most likely Be+white dwarf (WD) systems, predicted by the evolutionary models of massive binary systems but still not identified, according to the thermal nature of the X-rays (see discussion in Lopes de Oliveira et al. 2006).

In order to understand the nature of these objects and eventually unveil the mechanism leading to their unusual X-ray emission, compared to that of “normal” B/Be stars and known Be/X-ray systems, we have started an extensive X-ray and optical program intended to search for, and study new  $\gamma$  Cas analogs. Here we report on the X-ray properties of HD 110432 based on a campaign of three EPIC/XMM-Newton observations, along with optical observations. The HD 110432’s properties are discussed in the light of single-star and accreting binary models.

## 2. Previous observations of the main properties of HD 110432

### 2.1. Optical and UV properties

HD 110432 is a bright B1IVe star ( $V = 5.2$ ,  $B = 5.5$ ), located behind the Southern Coalsack, probable member of the open cluster NGC 4609 ( $\sim 60$  Myr; Codina et al. 1984; Feinstein & Marraco 1971; Kilkenny et al. 1985; Kharchenko et al. 2005; Smith & Balona 2006). The UV-to near IR spectrum and the Balmer jump of HD 110432 imply a  $T_{\text{eff}}$  of 25000 K and 22510 K, and  $\log g$  of 3.5 and 3.9, respectively (Codina et al. 1984; Zorec et al. 2005). Zorec et al. (2005) estimated a mass of  $9.6 M_{\odot}$  for the star. HD 110432 is not known to be in a binary system. Rotational velocity  $V_{\text{rot}} \sin i$  measures derived using different optical and UV lines vary from 300 to 400 km s $^{-1}$  (Slettebak 1982; Codina et al. 1984; Ballereau et al. 1995; Frémat et al. 2005; Smith & Balona 2006). For example, the He II  $\lambda 1640$  profile is similar in equivalent width and broadening to the feature in the  $\gamma$  Cas spectrum. High resolution spectra obtained of HD 110432 by Smith & Balona (2006) in 2005 January–February show that the He I  $\lambda 4471$ ,  $\lambda 5876$ , and  $\lambda 6678$  lines include strong wings extending to at least  $\pm 1000$  km s $^{-1}$ . The cause of these wings is unknown. Although single previous observation of  $\lambda 4471$  published by Ballereau et al. (1995) did not cover this full velocity range, it exhibits emission bumps to the blue and red of the line center that have not been reported in other spectra of the star. The He I and strong metallic

lines in the yellow-red region shows symmetrical emission peaks spaced  $\pm 100$  km s $^{-1}$  from line center. Metallic emission features were also reported in photographic spectra of  $\gamma$  Cas (Bohlin 1970). The kinematic separation and strengths of the peaks in HD 110432 indicate that the disk is viewed nearly edge on and that its mass and geometric extent are on the “high end” of what is typical for classical Be stars.

Both optical spectroscopic and photometric variability is also prevalent in HD 110432. Smith & Balona (2006) found that the He I  $\lambda 5876$  and  $\lambda 6678$  lines often exhibit “migrating sub-features” ( $msf$ ), which are quasi-absorption and emission bumps moving blue-to-red across the line profile. These appear in line profiles at irregular intervals and proceed across the profile with an acceleration near 100 km s $^{-1}$  hr $^{-1}$ . Such features have been observed by several authors in the  $\gamma$  Cas spectrum (Yang et al. 1988; Smith 1995; Smith & Robinson 1999).

A photometric period of either 1.77 or 1.42 days has been claimed for HD 110432 by Barrera et al. (1991) on the basis of 41 observations, but we cannot confirm this on the basis of photometric monitoring in 2002, as reported by Smith & Balona (2006). However, both the Cousins  $B$  and  $V$ -band light curves of this paper exhibited a clear  $\sim 3$ –4% sinusoidal modulation with a timescale of 130 days in 2002.

### 2.2. X-ray properties

BeppoSAX follow-up observations (Torrejón & Orr 2001) of some hard X-ray sources discovered in the HEAO-1 all-sky survey (Tuohy et al. 1988) revealed the unusual X-ray emission of HD 110432. The X-ray energy distribution was well described by a hot-thermal plasma model with  $kT \sim 11$  keV or by a *power law* model with photon index  $\Gamma \sim 1.63$  and a cut-off energy  $E_c \sim 19.9$  keV. This last model required additional Gaussian lines at 6.76 keV and 8.4 keV. The first line, with an EW of  $\sim 600$ –700 eV, was interpreted as an unresolved blend of the Fe XXV(6.7 keV) and Fe XXVI (6.97 keV) lines. As this feature is naturally predicted by the hot plasma model, a thermal interpretation of the X-ray emission was logically preferred. The BeppoSAX data did not show evidence for the presence of a fluorescent emission iron line at 6.4 keV. In the 2–10 keV band, the X-ray flux corrected for absorption ( $\sim 3.2 \times 10^{-11}$  erg cm $^{-2}$  s $^{-1}$ ) yields a luminosity of  $3.4 \times 10^{32}$  erg s $^{-1}$  if the distance to the system is 300 pc (Hipparcos; Perryman 1997). The X-ray spectrum of HD 110432 was affected by a hydrogen column of  $\sim 1.1$ – $1.4 \times 10^{22}$  cm $^{-2}$ , more than the  $\sim 2 \times 10^{21}$  cm $^{-2}$  value due to the Galactic reddening toward the star as derived from the colour excess ( $E(B-V) = 0.4$ ; Rachford et al. 2001). A single oscillation with a timescale of 14 ks was also suspected by Torrejón & Orr (2001). These authors concluded that HD 110432 was likely a high mass X-ray binary with an accreting WD companion. In their picture the X-ray variations were caused by rotational modulation of a hot

**Table 1.** Journal of XMM-Newton observations. In all cases the *thick* filter was applied to reject optical light, and the *pn* and MOS1-2 cameras were operated in the *extended full window* and *full window* modes, respectively.

Obs. ID	EPIC Cameras	Date	Start time	Duration (s)	Source counts <sup>a</sup> (cts s <sup>-1</sup> ) / (% of the events)	GTI <sup>b</sup> / % Obs. (ks)
0109480101 (OBS. 1)	<i>pn</i>	3 July 2002	T15:51:56	49398	2.726 / 98.2%	48600 / 98.4%
	MOS1		T15:00:31	52778	0.740 / 97.3%	52778 / 100%
	MOS2		T15:00:31	52778	0.994 / 97.2%	52778 / 100%
0109480201 (OBS. 2)	<i>pn</i>	26 August 2002	T21:55:14	44823	2.269 / 95.0%	23600 / 52.6%
	MOS1		T21:03:49	47827	0.911 / 95.8%	44600 / 93.2%
	MOS2		T21:03:50	47837	0.932 / 96.0%	44200 / 92.4%
0109480401 (OBS. 3)	<i>pn</i>	21 January 2003	T01:07:38	44391	1.913 / 97.2%	43400 / 97.8%
	MOS1		T00:16:20	47764	0.663 / 96.5%	47400 / 99.2%
	MOS2		T00:16:12	47772	0.644 / 96.9%	47700 / 99.8%

<sup>a</sup> data at 0.6–12 keV collected during all observation time, corrected on axis; <sup>b</sup> good time interval, after excluding times of enhanced soft-proton background: < 1 (and < 0.4) counts per second in the single-events *pn* (and MOS) light curve from whole camera, at E > 10 keV.

spot on this companion. Smith & Balona (2006) noted that the fluctuations causing this single modulation also occur in the light curve of  $\gamma$  Cas but these do not repeat regularly.

### 3. Observations

#### 3.1. Optical observations

We observed HD 110432 using the ESO Multi-Mode Instrument (EMMI) on the 3.5-m New Technology Telescope (NTT) at La Silla, Chile, on two occasions. On 5 June 2003, an H $\alpha$  spectrum was taken with the red arm in intermediate-resolution mode (REMD) and grating #6. The red arm is equipped with a mosaic of two thin, back-illuminated  $2048 \times 4096$  MIT/LL CCDs and this configuration results in a nominal dispersion of  $0.4\text{\AA}/\text{pixel}$  over the range  $\lambda\lambda 6440$ – $7150\text{\AA}$ . The resolution, measured from the widths of arc lines, is  $\sim 1.2\text{\AA}$ . The blue spectrum was taken with the blue arm in intermediate-resolution mode (BLMD) and grating #12. The blue arm is equipped with a Textronik TK1034 thinned, back-illuminated  $1024 \times 1024$  CCD and this configuration results in a nominal dispersion of  $0.9\text{\AA}/\text{pixel}$  over the range  $\lambda\lambda 3820$ – $4750\text{\AA}$ . The resolution, measured on arc lines, is  $\sim 2.6\text{\AA}$ .

On 10 May 2004, we observed the H $\alpha$  region with the same configuration, but a slightly different grating angle, resulting in coverage of the  $\lambda\lambda 6170$ – $6880\text{\AA}$  range. The blue spectrum was taken with the red arm in exactly the same configuration, but using grating #7 instead. (The red arm has lower efficiency in the blue, but grating #7 allows a much better compromise between resolution and range than any blue grating). The spectrum covers the range  $\lambda\lambda 3800$ – $5200\text{\AA}$ , with a nominal dispersion of  $0.85\text{\AA}/\text{pixel}$  and a measured resolution of  $\sim 2.5\text{\AA}$ .

Image pre-processing was carried out with *MIDAS* software, while data reduction was achieved with the *Starlink* packages *CCDPACK* (Draper et al. 2000) and *FIGARO* (Shortridge et al. 1997).

#### 3.2. X-ray observations

HD 110432 was serendipitously observed in a campaign of three XMM-Newton exposures of the Wolf-Rayet star WR 47 (see Table 1 for details). Its extreme off-axis position (in the range of  $13'$ ) does not allow it to be in the field of view of the high-resolution RGS cameras. Only the medium-resolution ( $E/\Delta E \sim 20$ – $50$ ) EPIC cameras (MOS1, MOS2, and *pn*) were able to detect HD 110432 in its fields, which cover an area of  $\sim 700$  arcmin $^2$  in the used observational modes (*extended full window* for *pn*, and *full window* for MOS1 and MOS2). The observations were taken on 3 July 2002 (hereafter OBS. 1), 26 August 2002 (OBS. 2), and 21 January 2003 (OBS. 3).

We use the *Science Analysis Software* (SAS) v6.5 and the most recent calibration files for the data processing. The spectral analysis was performed with XSPEC v11.3.1.

In the following only single and double event patterns ( $\leq 4$ ), and single to quadruple event patterns ( $\leq 12$ ) were used for *pn* and MOS cameras, respectively. The only exception is in evaluating the parameters of the iron lines (Table 4 and Fig. 3) in which only single-*pn* events collected during the whole observation were used in order to obtain the best possible energy resolution ( $\sim 150$  eV at 6.4 keV)<sup>1</sup>. According to the *epatplot*/SAS task, the data are not affected by photon pile up.

Only a few time intervals were affected by slightly enhanced background of solar particles (Table 1). We exclude photons collected during these intervals when investigating the spectral energy distribution, and we use the whole observations for the timing analysis and investigation of parameters of the Fe K $\alpha$  complex.

There is a residual shoulder around 0.3 keV in the spectra which could be due to bad cancellation of a strong absorption feature present in the thick filter. For that reason, we preferred to discard the low energy part of the spectrum below 0.6 keV. The backgrounds were extracted in

<sup>1</sup> XMM-Newton User's Handbook

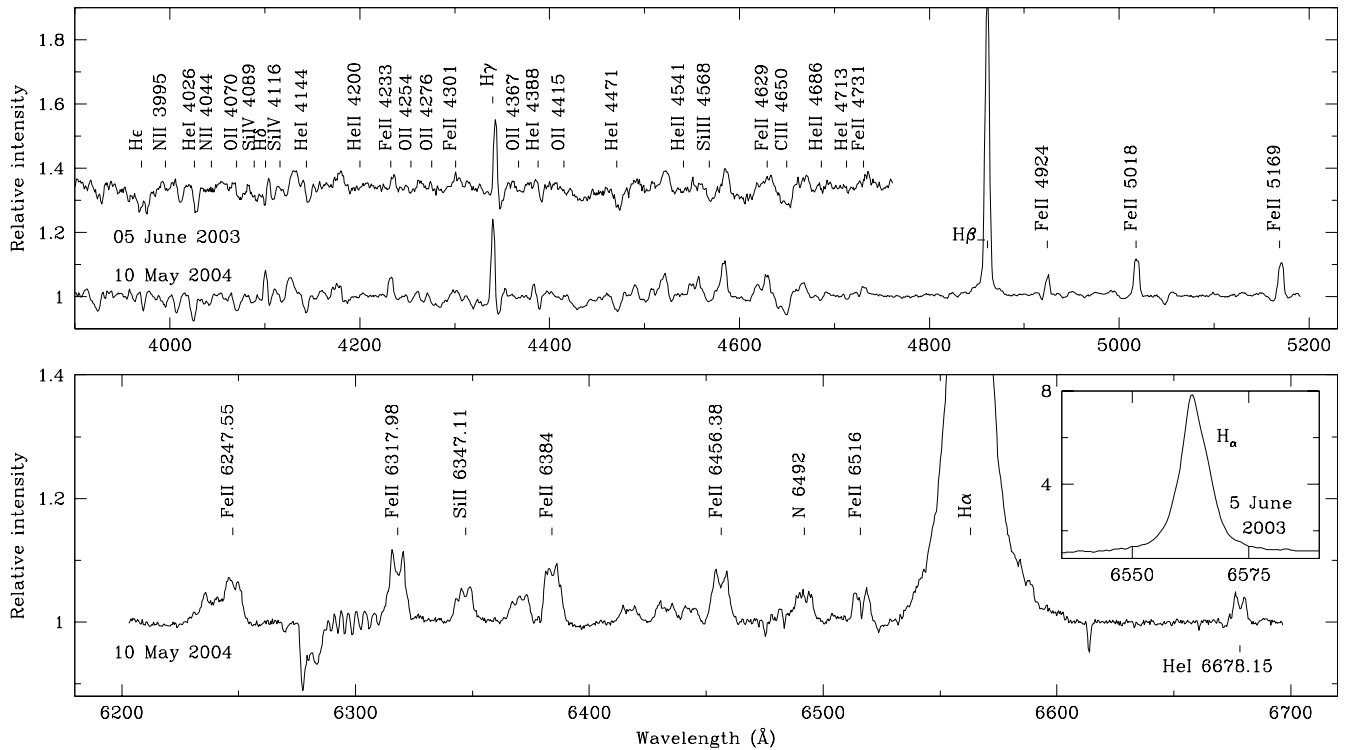


**Fig. 1.** Blue and red optical spectra of HD 110432. The inset shows the profile of the H $\alpha$  line.

large regions located in the same CCD as the source. For spectral studies, the energy channels of each camera were grouped in bins containing at least 150 events, and the PHABS model was applied to account for the photoelectric absorption.

Throughout this paper, we use data collected by all EPIC cameras (MOS1, MOS2, and *pn*) in timing analysis, but owing to possible uncertainties in the cross-calibration between the three cameras at large off-axis angle we opted to use only the *pn* data for spectral studies. We checked that the lower S/N MOS data yielded spectral parameters consistent with those derived from the EPIC *pn*.

#### 4. Optical properties

There are numerous metallic emission lines in the blue and red spectra of HD 110432 (Fig. 1), chiefly arising from Fe II transitions, in addition to strong H-Balmer lines. As inferred of a number of Be stars (Slettebak et al. 1992), the detection of these lines in HD 110432 suggests the presence of a dense and/or large circumstellar disk, and according to the double-peak feature of the metallic lines, in a nearly edge-on orientation. We derive an equivalent width (EW) of  $-60 \pm 1 \text{ Å}$  for the H $\alpha$  line.

Interestingly, the double-lobe emissions of the metallic lines seem more equal in Fig. 1 than those obtained by Smith & Balona (2006), in which on average the blue component was slightly stronger, and we speculate the existence of some kind of instability in the HD 110432's disk - most likely an one-arm disk instability (e.g. Okazaki 1991).

The presence of the emission lines renders difficult the identification of weak absorption features, and therefore the determination of the spectral type and luminosity class. The spectral type can be estimated from the presence of a moderately strong Si IV 4089 $\text{\AA}$  line and a weak He II 4686 $\text{\AA}$  line to be close to B0.5-1, while the relative strength of the complex around C III 4650 $\text{\AA}$  suggests that it is likely to be a moderately luminous star. Thus, we conclude that the luminosity class of HD 110432 is compatible with III or IV.

### 5. The spectral energy distribution in X-rays

#### 5.1. The average spectra

The XMM-Newton observations of HD 110432 were investigated separately for each epoch (as Table 1). The star exhibits a hard X-ray spectrum, in which a Fe K $\alpha$  complex in emission – composed by a fluorescent feature at 6.4 keV, Fe XXV (He-like) at 6.7 keV, and Fe XXVI (H-like) at 6.97 keV lines – is clearly detected in all observations. In addition, a Fe XXVI Ly $\beta$  line seems to be present in two of the three observations. The fluorescent line should be produced in a dense-cold medium close and in the line-of-sight of the X-ray source, or over the surface of a putative accreting WD companion. Moreover, the highly ionized iron lines supports a thermal nature, at least dominantly, of the X-ray emission.

Models with one or two thermal components do not give acceptable results. Replacing one of the thermal component by a *power law*, even though including a high en-

**Table 2.** Best-fit parameters for the X-ray spectrum of HD 110432 in each XMM-Newton observation from a 3-thermal model.

	OBS. 1	OBS. 2	[OBS. 2]	OBS. 3
M1: $N_{\text{H}} \times (T_1 + T_2 + T_3 + 2 \text{ G. LINES})$				
$N_{\text{H}_a}$ ( $10^{22} \text{ cm}^{-2}$ )	$0.34^{+0.01}_{-0.01}$	$0.42^{+0.05}_{-0.04}$	$[0.46^{+0.04}_{-0.04}]$	$0.44^{+0.02}_{-0.02}$
$kT_1$ (keV)	$0.66^{+0.05}_{-0.05}$	$0.37^{+0.07}_{-0.15}$	$[0.30^{+0.07}_{-0.04}]$	$0.66^{+0.26}_{-0.09}$
$f_{T_1}$ ( $\text{erg cm}^{-2} \text{ s}^{-1}$ )	$7.8 \times 10^{-13}$	$1.1 \times 10^{-12}$	$[2.7 \times 10^{-12}]$	$5.2 \times 10^{-13}$
$\text{EM}_{T_1}$ ( $10^{55} \text{ cm}^{-3}$ )	0.03	0.04	[0.1]	0.02
$kT_2$ (keV)	$5.40^{+0.60}_{-0.81}$	$3.49^{+1.12}_{-0.91}$	$[1.55^{+0.37}_{-0.22}]$	$5.68^{+3.80}_{-1.01}$
$f_{T_2}$ ( $\text{erg cm}^{-2} \text{ s}^{-1}$ )	$9.1 \times 10^{-12}$	$5.5 \times 10^{-12}$	$[1.4 \times 10^{-12}]$	$7.9 \times 10^{-12}$
$\text{EM}_{T_2}$ ( $10^{55} \text{ cm}^{-3}$ )	0.5	0.3	[0.09]	0.4
$kT_3$ (keV)	$27.17^{+3.61}_{-4.01}$	$20.82^{+4.67}_{-3.80}$	$[14.26^{+1.95}_{-1.28}]$	$36.86^{+7.24}_{-7.68}$
$f_{T_3}$ ( $\text{erg cm}^{-2} \text{ s}^{-1}$ )	$3.7 \times 10^{-11}$	$3.2 \times 10^{-11}$	$[3.7 \times 10^{-11}]$	$3.1 \times 10^{-11}$
$\text{EM}_{T_3}$ ( $10^{55} \text{ cm}^{-3}$ )	1.9	1.7	[1.9]	1.7
$Z_{T_3}$ ( $Z_{\odot}$ )	$0.31^{+0.12}_{-0.09}$	$0.45^{+0.13}_{-0.12}$	$[0.44^{+0.08}_{-0.08}]$	$0.52^{+0.18}_{-0.17}$
Line (keV)	$6.39^{+0.04}_{-0.01}$	$6.41^{+0.02}_{-0.02}$	$[6.41^{+0.02}_{-0.02}]$	$6.4^b$
$\sigma_{\text{Line}}$ (keV)	< 0.05	0.01 <sup>b</sup>	[0.01 <sup>b</sup> ]	0.01 <sup>b</sup>
Line (keV)	8.2 <sup>b</sup>	...	...	$8.16^{+0.08}_{-0.06}$
$\sigma_{\text{Line}}$ (keV)	< 0.11	...	...	< 0.12
$f_{\text{tot}}$ ( $\text{erg cm}^{-2} \text{ s}^{-1}$ )	$4.8 \times 10^{-11}$	$3.9 \times 10^{-11}$	$[4.1 \times 10^{-11}]$	$4.2 \times 10^{-11}$
$\chi^2/\text{d.o.f.}^a$	1.05/588	1.13/270	[1.13/270]	1.00/386

<sup>a</sup> degrees of freedom; <sup>b</sup> frozen parameter.

Notes: solar abundances for  $T_1$  and  $T_2$ . Fluxes are given unabsorbed in the 0.2–12 keV energy band. Quoted errors are at the 90% confidence level.

ergy cut-off, does not improve the quality of the fits. These models do not account simultaneously for the observed excess in the hard X-ray continuum and intensities of the He and H like iron lines, even if each component is affected for different absorption columns. Likewise, the fits are not much improved by the addition of a second absorption for the hard component.

X-ray spectra are better described by the sum of three thermal components (3-T): a *cool* ( $kT_1 \sim 0.4\text{--}0.7$  keV), a *warm* ( $kT_2 \sim 3\text{--}6$  keV), and a *hot* plasma ( $kT_3 \sim 21\text{--}37$  keV; see M1 in Table 2). About 80% of the 0.2–12 keV flux is due to the *hot* plasma, notably as for  $\gamma$  Cas (Smith et al. 2004), while the *warm* and *cool* plasmas account for the other  $\sim 18\%$  and  $\sim 2\%$ , respectively. The same distribution is followed by the emission measure of each thermal component, with respect to the total value. The column density is larger than that due to the interstellar medium, and the local absorptions increase for each of the subsequent observations. The Ly $\beta$  line, suspected in OBS. 1 and OBS. 3, cannot be reproduced by any thin thermal MEKAL model we have tested, and a gaussian line was added. A second gaussian line accounts for the Fe fluorescence line at 6.4 keV.

In OBS. 1 and OBS. 3 the fitting process following the model M1 converges toward a unique solution. In OBS. 2, however, the fitting process finds two equally probable configurations with quite different temperature for the three components, as well as different flux contributions and emission measures for the *cool* and *warm* components (Table 2). It seems, however, that the models with the highest temperatures provides a better description of the

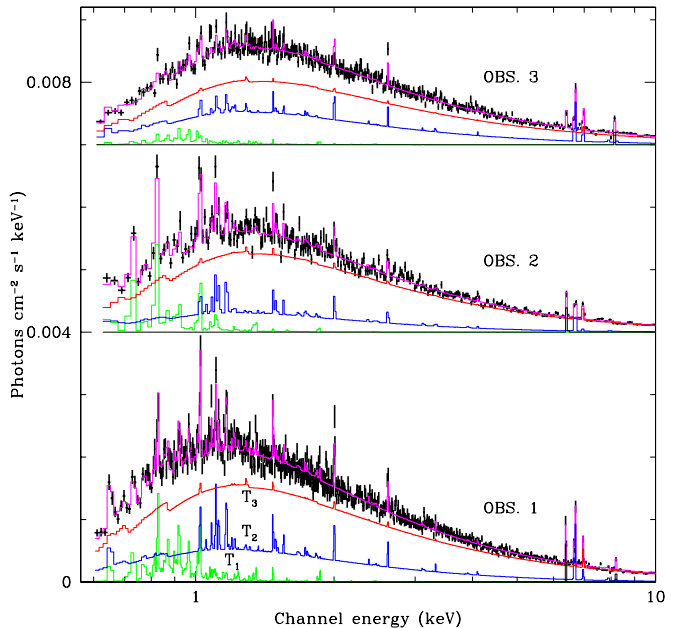


**Fig. 2.** Unfolded X-ray spectra at different epochs, added to constant values for clarity (as M1 in Table 2).

iron line complex. In the “colder convergence” for OBS. 2, the *cold* and *warm* plasma account for 4% each of the total value, and  $\sim 6.5\%$  and  $\sim 3.5\%$ , respectively, of the total 0.2–12 keV flux – in contrast with those contributions of the “hotter convergence” for OBS. 2 and values derived from the other observations, summarized above.

**Table 3.** Best-fit parameters for the X-ray spectrum of HD 110432 in each XMM-Newton observation, from thermal models added to a *power law* component.

	OBS. 1	OBS. 2	OBS. 3
M2: $N_{\text{Ha}} * T_1 + N_{\text{Hb}} * (T_2 + \text{P. LAW} + 2 \text{ G. LINES})$			
$N_{\text{Ha}}$ ( $10^{22} \text{ cm}^{-2}$ )	$0.92^{+0.31}_{-0.31}$	$0.74^{+0.19}_{-0.19}$	$1.10^{+1.29}_{-0.62}$
$kT_1$ (keV)	$0.22^{+0.04}_{-0.03}$	$0.35^{+0.13}_{-0.10}$	$0.21^{+0.16}_{-0.10}$
$f_{T_1}$ ( $\text{erg cm}^{-2} \text{ s}^{-1}$ )	$3.9 \times 10^{-11}$	$4.1 \times 10^{-12}$	$2.7 \times 10^{-11}$
$\text{EM}_{T_1}$ ( $10^{55} \text{ cm}^{-3}$ )	1.8	0.2	1.3
$N_{\text{Hb}}$ ( $10^{22} \text{ cm}^{-2}$ )	$0.37^{+0.03}_{-0.02}$	$0.39^{+0.04}_{-0.03}$	$0.44^{+0.03}_{-0.03}$
$kT_2$ (keV)	$8.76^{+0.75}_{-0.82}$	$10.24^{+1.58}_{-1.46}$	$9.34^{+1.42}_{-0.99}$
$f_{T_2}$ ( $\text{erg cm}^{-2} \text{ s}^{-1}$ )	$3.2 \times 10^{-11}$	$3.0 \times 10^{-11}$	$2.6 \times 10^{-11}$
$\text{EM}_{T_2}$ ( $10^{55} \text{ cm}^{-3}$ )	1.7	1.6	1.4
$Z_{T_2}$ ( $Z_{\odot}$ )	$0.43^{+0.05}_{-0.06}$	$0.42^{+0.17}_{-0.10}$	$0.50^{+0.39}_{-0.07}$
$\Gamma$	$1.09^{+0.15}_{-0.22}$	$1.04^{+0.79}_{-3.09}$	$1.02^{+0.23}_{-1.03}$
$f_{\Gamma}$ ( $\text{erg cm}^{-2} \text{ s}^{-1}$ )	$1.5 \times 10^{-11}$	$8.0 \times 10^{-12}$	$1.5 \times 10^{-11}$
Line (keV)	$6.39^{+0.03}_{-0.02}$	$6.41^{+0.02}_{-0.02}$	6.4
$\sigma_{\text{Line}}$ (keV)	<0.06	<0.07	0.01
Line (keV)	8.2 <sup>a</sup>	...	$8.16^{+0.07}_{-0.06}$
$\sigma_{\text{Line}}$ (keV)	0.0001 <sup>a</sup>	...	<0.11
$f_{\text{tot}}$ ( $\text{erg cm}^{-2} \text{ s}^{-1}$ )	$8.6 \times 10^{-11}$	$4.2 \times 10^{-11}$	$6.8 \times 10^{-11}$
$\chi^2/\text{d.o.f.}$	1.07/588	1.17/268	1.01/385
M3: $N_{\text{H}} * (\text{CEMEKL} + \text{P. LAW} + 2 \text{ G. LINES})$			
$N_{\text{H}}$ ( $10^{22} \text{ cm}^{-2}$ )	$0.34^{+0.01}_{-0.01}$	$0.38^{+0.01}_{-0.02}$	$0.45^{+0.01}_{-0.01}$
$T_{\text{max}}$ (keV)	$27.90^{+7.90}_{-4.98}$	$35.20^{+10.93}_{-8.33}$	$29.51^{+13.92}_{-6.45}$
$Z$ ( $Z_{\odot}$ )	$0.53^{+0.10}_{-0.08}$	$0.55^{+0.11}_{-0.06}$	$0.58^{+1.56}_{-0.09}$
$f_{\text{T}}$ ( $\text{erg cm}^{-2} \text{ s}^{-1}$ )	$3.7 \times 10^{-11}$	$3.6 \times 10^{-11}$	$3.2 \times 10^{-11}$
$\Gamma$	$1.13^{+1.79}_{-0.23}$	1.1 <sup>a</sup>	$1.04^{+2.48}_{-0.76}$
$f_{\Gamma}$ ( $\text{erg cm}^{-2} \text{ s}^{-1}$ )	$1.1 \times 10^{-11}$	$3.0 \times 10^{-12}$	$1.1 \times 10^{-11}$
Line (keV)	6.4 <sup>a</sup>	$6.41^{+0.02}_{-0.02}$	6.4 <sup>a</sup>
$\sigma_{\text{Line}}$ (keV)	0.01 <sup>a</sup>	< 0.07	0.01 <sup>a</sup>
Line (keV)	$8.20^{+0.12}_{-0.09}$	...	$8.16^{+0.06}_{-0.05}$
$\sigma_{\text{Line}}$ (keV)	0.01 <sup>a</sup>	...	0.01 <sup>a</sup>
$f_{\text{tot}}$ ( $\text{erg cm}^{-2} \text{ s}^{-1}$ )	$4.8 \times 10^{-11}$	$3.9 \times 10^{-11}$	$4.3 \times 10^{-11}$
$\chi^2/\text{d.o.f.}$	1.12/592	1.17/272	1.05/389

<sup>a</sup> degrees of freedom; <sup>b</sup> frozen parameter.

Notes: M2: solar abundances for  $T_1$ . M3:  $\alpha = 1$ . Fluxes are given unabsorbed in the 0.2–12 keV energy band. Quoted errors are at the 90% confidence level.

Contrary to the *warm* and *cool* components, in which the fits result in abundances which are consistent with solar values for all elements, sub-solar abundances are clearly needed for the model parameters of the *hot* component. Using the VMEKAL model, we checked that setting a lower Fe abundance for the *hot* component while keeping the abundances of other metals to their solar values gives results consistent with those obtained by freeing the elemental abundances altogether ( $Z \lesssim 0.5Z_{\odot}$ ). Therefore, except for the Fe, there is no reason to invoke nonsolar abundances for the *hot* plasma components.

So distinct temperatures strongly suggest complex X-ray environments. In this sense, we tried a number of 3-T models in which we:

- (a) - determined two absorption columns, one for the *hot* component and another for the *warm & cool* components;
- (b) - divided the *hot* plasma in (a) into two unequal sub-components. The absorption of the first subcomponent is determined independently of the absorption of the other subcomponent, which is tied to the *warm* and *cool* components. The relative fractions of the two *hot* components is determined as a free parameter;
- (c) - repeated the (b) model but forced the emission measures of the two *hot* subcomponents to be equal.

The models (a,b,c) do not improve the fits obtained from M1, and with two exceptions the derived parameters are consistent with those of M1 at the 90% confidence level. The two exceptions concern the *hot* component and its absorption following the model (b). According to this model,  $\sim 15$ –50% of the hottest component is more strongly absorbed ( $\sim 10 \times$ ) than the other  $\sim 50$ –85%. The latter *hot* subcomponent is tied to the absorption column of the *warm* and *cool* components, and the parameters for this column are consistent with those derived from M1 (see Table 2). Therefore, we can speculate that, similar to the X-ray spectrum of  $\gamma$  Cas (Smith et al. 2004), the hottest component of HD 110432 is affected by multiple absorption columns. As a second exception, the *hot* temperatures in each observation are systematically cooler than those of M1 by about 30%. We also note that the (a,b,c) models result in two convergences for OBS. 2. Both are consistent with those obtained from M1 in Table 2. The results of the models briefly discussed above corroborates the complex nature of the X-ray spectrum of HD 110432, already inferred from the simplified model M1.

As an alternative to the 3-T models discussed above, a good description of the observed X-ray energy distribution of HD 110432 is also obtained using a model composed of two thermal components (a *cool*,  $kT \sim 0.2$ –1.6 keV, and a *hot*,  $kT \sim 8$ –12 keV) added to a *power law* with a hard photon index (see Table 3). As in the 3-T model, the Fe XXV and Fe XXVI lines are well fitted by the thermal plasma model, and subsolar abundances, at least for Fe, are needed. In the 3-T model the iron lines arise from a combination of the *hot* ( $kT \sim 20$  keV) and *warm* ( $kT \sim 4$  keV) plasmas. The high temperature of the *hot* component is essentially required by the shape of the continuum. In the 2-T + PL model, the *power law* accounts for part of the hard X-ray continuum ( $\sim 20\%$  of the total 0.2–12 keV flux in all observations) and the iron lines can then be well represented by a single thermal component of temperature ( $kT \sim 10$  keV) intermediate between those of the *warm* and *hot* plasmas in the 3-T model, and consistent with that obtained by Torrejón & Orr (2001). The flux contributions of the *hot* plasma is about  $\sim 55\%$  of the total 0.2–12 keV flux in OBS. 1,  $\sim 70\%$  in OBS. 2, and  $\sim 40\%$  in OBS. 3.

**Table 4.** Parameters of the iron emission lines detected in X-rays.

	OBS. 1			OBS. 2			OBS. 3		
	$E_C$ (keV)	EW (eV)	Flux <sup>a</sup> ( $\times 10^{-5}$ )	$E_C$ (keV)	EW (eV)	Flux <sup>a</sup> ( $\times 10^{-5}$ )	$E_C$ (keV)	EW (eV)	Flux <sup>a</sup> ( $\times 10^{-5}$ )
Fe K	$6.40^{+0.01}_{-0.04}$	$47.8^{+11.9}_{-14.0}$	$1.9^{+0.5}_{-0.5}$	$6.42^{+0.02}_{-0.02}$	$48.7^{+16.3}_{-11.4}$	$1.5^{+0.5}_{-0.3}$	$6.46^{+0.01}_{-0.03}$	$54.2^{+11.8}_{-12.1}$	$1.9^{+0.4}_{-0.4}$
Fe XXV	$6.70^b$	$159.0^{+34.3}_{-20.2}$	$5.8^{+1.2}_{-0.7}$	$6.68^{+0.01}_{-0.01}$	$126.0^{+18.4}_{-16.2}$	$3.7^{+0.5}_{-0.5}$	$6.67^{+0.05}_{-0.03}$	$86.9^{+88.0}_{-21.7}$	$3.0^{+3.1}_{-0.7}$
Fe XXVI Ly $\alpha$	$6.97^b$	$60.8^{+19.0}_{-23.8}$	$2.1^{+0.7}_{-0.8}$	$6.97^{+0.01}_{-0.01}$	$99.1^{+14.7}_{-13.6}$	$2.6^{+0.4}_{-0.4}$	$6.94^{+0.11}_{-0.05}$	$121.0^{+40.1}_{-75.8}$	$3.6^{+1.2}_{-2.3}$
Fe XXVI Ly $\beta$ (?)	$8.18^{+0.03}_{-0.01}$	$109.0^{+41.2}_{-33.2}$	$2.2^{+0.8}_{-0.7}$	...	...	...	$8.14^{+0.02}_{-0.02}$	$152.0^{+42.8}_{-33.0}$	$2.9^{+0.8}_{-0.6}$

<sup>a</sup> total flux in line, in units of photons cm $^{-2}$  s $^{-1}$ ; <sup>b</sup> frozen parameter.

Notes: EWs estimated from a PHABS\*(BREMSS+3 GAUSSIAN LINES) model applied to spectra in the 5–10 keV energy range.  $E_C$  are the centroids of the Gaussian lines. Quoted errors are at 1  $\sigma$ .

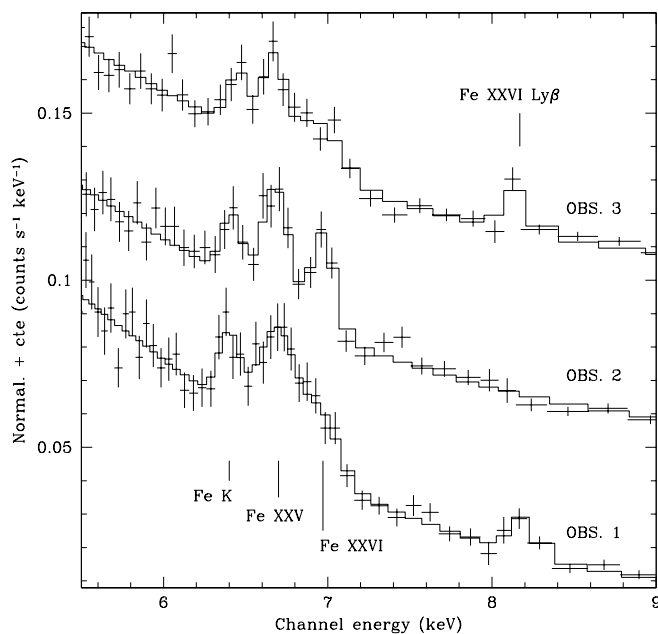


**Fig. 3.** The Fe K $\alpha$  complex and the suspected Fe XXVI Ly $\beta$  line of HD 110432 seen in different epochs. The *pn* single-spectra are shown normalized and added to a constant term for clarity. See EWs in Table 4.

We tried the CEMEKL<sup>2</sup> model, largely used in cataclysmic variables systems (CVs) leaving the  $\alpha$  parameter free. The fit converges towards  $\alpha$  values of 1, in agreement with the adiabatic case. The resulting temperatures  $kT_{max}$  in the three observations range from 40 to 60 keV. However, this model gives slightly larger  $\chi^2_\nu$  than those of models discussed above for two observations ( $\chi^2_\nu=1.14$ , 1.15, and 1.06, for OBS. 1, 2, and 3, respectively). It also predicts Fe XXVI and Fe XXV lines more and less strong than observed, respectively, and on this basis can probably be excluded. The bad fit quality achieved by the CEMEKL model to describe the ionized Fe XXV and Fe XXVI lines

<sup>2</sup> A multi-temperature emission model built from the MEKAL code – emission continuum/line spectrum from hot diffuse gas –, in which the emission measures of the plasmas follow a power-law in temperature:  $EM \propto (T/T_{max})^\alpha$ .

indicates that the 3-T description is most likely not the approximation of a spectrum emitted by a single region with a continuously variable temperature distribution, but rather reflects the existence of three physically separated sites of emission.

The addition of a *power law* component to the CEMEKL model improves the fits – due the better description of the high energy part of the spectrum – but it does not provide mean  $\chi^2_\nu$  values as low as those given by the 3-T model (see Table 3). We also tried a CEMEKL + soft thermal component to test the idea that part of the softest emission could arise in the shocked wind of the early type star. Again, the fit is improved but remains significantly worse than that of the 3-T model, essentially due to the inability to represent the details of the iron complex emission.

From the 3-T model shown in Table 2 the unabsorbed flux in the 2–10 keV energy band is  $\sim 2.3$ – $2.9 \times 10^{-11}$  erg cm $^{-2}$  s $^{-1}$  in the XMM-Newton observations. This value is slightly lower than those obtained by BeppoSAX ( $\sim 3.2 \times 10^{-11}$  erg cm $^{-2}$  s $^{-1}$ ; Torrejón & Orr 2001) and HEAO-1 ( $\sim 4.7 \times 10^{-11}$  erg cm $^{-2}$  s $^{-1}$ ; Tuohy et al. 1988) satellites. Assuming a distance of  $d = 300$  pc to HD 110432 (Perryman 1997), implies a luminosity of  $\sim 2.6$ – $3.1 \times 10^{32}$  erg s $^{-1}$ . In the 0.2–12 keV band, the unabsorbed XMM-Newton flux is about  $3.9$ – $4.8 \times 10^{-11}$  erg cm $^{-2}$  s $^{-1}$ , or  $L_x \sim 4.2$ – $5.2 \times 10^{32}$  erg s $^{-1}$  for  $d = 300$  pc (Table 2).

## 5.2. The parameters of the iron lines in emission

The lines of the Fe K $\alpha$  complex are the strongest resolved emission lines in the 0.2–12 keV spectrum of HD 110432, and all are clearly present in each XMM-Newton observation (Fig. 3). In evaluating the parameters of the iron lines, a thermal bremsstrahlung model was used to describe the 5–10 keV continuum, and four Gaussian lines were added to represent each of the fluorescence, Fe XXV, Fe XXVI, and the suspected Fe XXVI Ly $\beta$  lines.

Table 4 lists the equivalent width of each Fe component in each observation. The flux of the fluorescence line seems to be constant. On the other hand, the relative fluxes of each ionized component are slightly different in each epoch (Fig. 3 and Table 4), but their EWs are still mutually con-

**Table 5.** Temperatures from the Fe lines and hard X-ray continuum in the framework of 1-T model, and Fe abundance.

	$kT_{ion}^a$ (keV)	$Z_{Fe}^a$ ( $\times$ solar)	$kT_{h,cont}^b$ (keV)
OBS. 1	$8.74^{+0.86}_{-0.78}$	$0.23^{+0.06}_{-0.02}$	$17.76^{+4.46}_{-4.22}$
OBS. 2	$10.68^{+1.76}_{-1.63}$	$0.27^{+0.09}_{-0.08}$	$15.29^{+5.37}_{-3.56}$
OBS. 3	$9.87^{+1.46}_{-1.06}$	$0.26^{+0.07}_{-0.06}$	$24.62^{+9.68}_{-4.89}$

<sup>a</sup> based in the Fe XXV and Fe XXVI lines, using the 6–8 keV energy range; <sup>b</sup> from the 4–6 keV + 8.4–12 keV continuum.

Notes: Quoted errors are at the 90% confidence level.

sistent at  $1\sigma$ . An apparent decrease is suspect for the He-like flux in each successive observation, while the contrary is the case for the H-like ion.

The suspected presence of the Fe XXVI Ly $\beta$  line at 8.2 keV is a novelty for spectra of any high-mass stellar X-ray source, whether emitted in the environs of the massive star or in a high-mass accretion binary system. Although the theory for the formation of this feature is not yet well developed in the literature, one can make a few simple statements from what is known about the recombination spectrum of lighter hydrogenic ions. First, the Ly $\beta$  to Ly $\alpha$  strength ratio of such ions increases with temperature, but rather only slowly so. For example, we have found that the Ly $\beta$ /Ly $\alpha$  line intensity ratio cannot be reproduced by any thin thermal mekal model. We also believe that the clear differences in the Ly $\beta$  ratio noted in Fig. 3 between OBS. 2 and OBS. 1 cannot be explained through the Boltzmann effect for the change in temperature,  $\sim 21$  keV to 27 keV, respectively see (see e.g. Smith et al. 2001). Changes in this ratio are more likely caused by a transition to a mildly optically thick regime, wherein the Ly $\alpha$  strength would be depressed through saturation. Alternatively, a suppressed emission of Ly $\alpha$  could be caused by the superposition of some absorption due to resonance scattering – this would hint at a change in geometry of the plasma components. In either of the latter two alternatives, we might expect to see a difference in the derived iron abundance in OBS. 2 relative to the other two observations. However, as shown in Table 5, any such effect must be small because the Fe abundances found for the three observations are internally consistent. While we still believe either of the latter two options offers a viable resolution of the problem, we must leave this as an unresolved issue.

### 5.3. The iron lines in emission and the hard continuum

We applied the CEVMKL<sup>3</sup> model in the 6–8 keV energy range, in each observation, in order to estimate the ionization temperature ( $kT_{ion}$ ) and iron abundance ( $Z_{Fe}$ ) required by the Fe XXV and Fe XXVI lines. Using the same model in the 4–6 + 8.4–12 keV energy range, we also esti-

<sup>3</sup> A CEMEKL-like model, in which the abundance of each element is allowed to vary.

mate the temperature ( $kT_{h,cont}$ ) needed to describe only the hard continuum.

The results are shown in Table 5. This analysis strongly suggests that  $kT_{h,cont} > kT_{ion}$ , even though for OBS. 2 at the 90% confidence level. The iron abundance, in all observations, is consistent with  $0.25 \times Z_{Fe,\odot}$ .

## 6. Timing behavior of the X-ray emission

Figure 4 shows background- and barycentric-corrected light curves of HD 110432 in each XMM-Newton observation. We plot the light curves in the 0.6–2 keV and 2–12 keV energy bands, chosen to give comparable count rates, and the corresponding hardness ratio.

At all epochs the source shows strong intensity and hardness variations, in which ubiquitous flare are observed. The dotted lines in Figure 4 represents the  $1\sigma$  confidence belts derived from the photon statistic of 10 consecutive time bins of 150 s each. Interestingly, as for  $\gamma$  Cas (Smith et al. 1998a), the shots in HD 110432 are clearly superimposed over a slowly varying basal flux, and they are detected in time scales as short as 10 s, a limit determined by photon statistics.

There is no evidence for a hardness-intensity correlation in HD 110432 (Fig. 5). But there are some noticeable features. First, the average (absorbed) intensity seems to decrease over the subsequent observations and is accompanied by a slight increase of the spectral hardness. Second, the dispersion of the hardness ratio distribution is more accentuated in the second and third observations. Finally, rapid hardness variability reveals that the X-ray energy distribution varies on short time scales.

### 6.1. Investigating the soft and hard states

The strong and rapid variations, clearly observed in the light curves of HD 110432, are accompanied by a similar behaviour of the hardness ratios (hereafter HR; Figure 4). The changes are apparently random and occur on time scales as short as tens of seconds.

In order to try to investigate the detailed nature of the spectral variability of HD 110432, we went on to study spectra accumulated during times of soft (S) and hard (H) dominated emission. The corresponding HR limits were adopted as being smaller than 0.9 and larger than 1.1 times the mean HR for the “soft” and “hard” spectra, respectively. These limits are shown by dashed lines in Figures 4 and 5. The times associated to the soft and hard states can be seen in the bottom of the each lower panel of Figure 4, of which were excluded those associated to enhanced solar-proton background.

Figure 6 shows the counts spectra accumulated in the soft and hard states, and the resulting fits. The best-fit parameters are shown in Table 6. A soft photon deficit is clearly seen in the hard state and in observations 2 and 3 is accompanied by an increase of the flux of hard photons above  $\sim 2$  keV. In the framework of the 3-T model, it seems that most of the differences between the hard

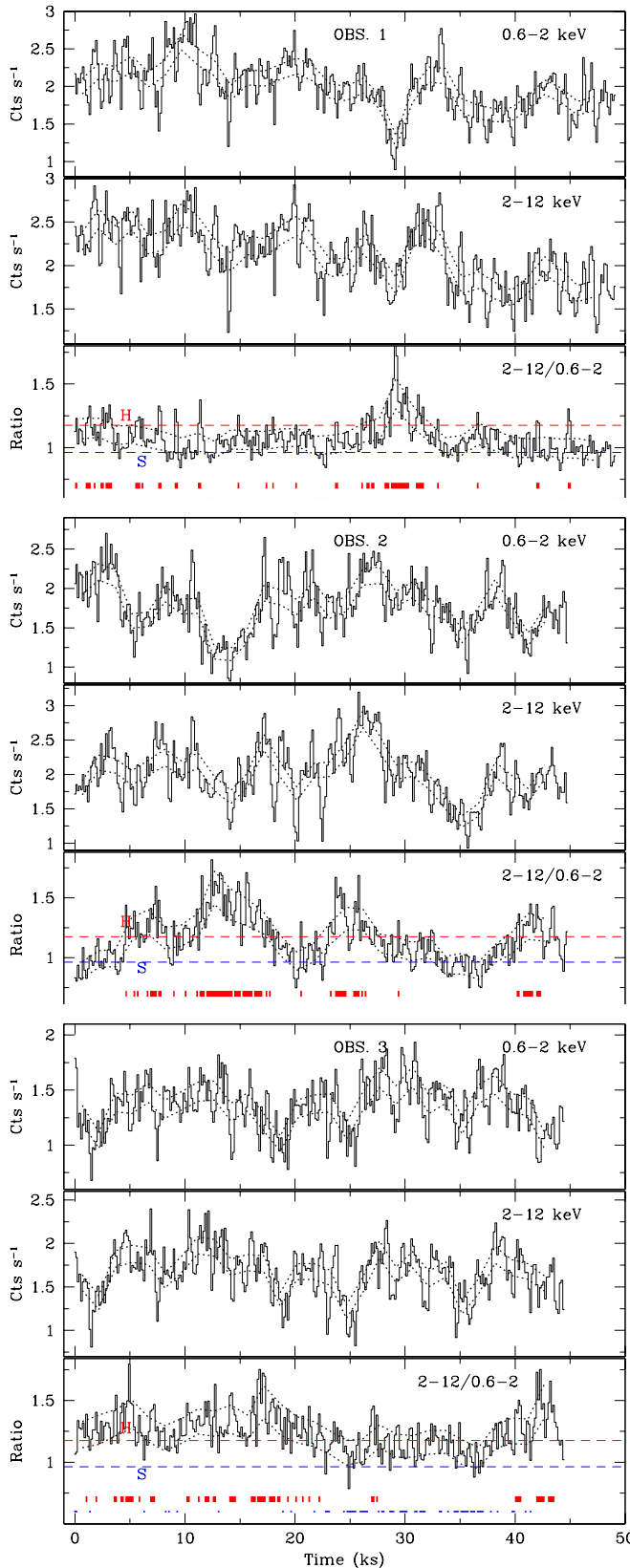


**Fig. 4.** EPIC light curves and hardness variabilities. Time bins of 150 s. Dashed lines indicate the limits of the adopted hard (H) and soft (S) states. The segment of lines in the bottom of the lower panels show the H and S time intervals. Dotted lines represent the  $1\sigma$  confidence belts (see text).

and the soft states are due to a change in the column density and in the luminosity of the *cool* and *warm* components. However, the temperatures of the *cool* and *warm* components are not statistically different in the hard and soft states and the direction of their evolution with state varies with the observation considered. The mean unabsorbed flux of the highest temperature component remains about the same in the hard and soft states of OBS. 1 and OBS. 3 while a flux increase ( $\sim 40\%$ ) occurs in OBS. 2.

## 6.2. Search for coherent pulsations

We searched for coherent pulsations using the  $Z_n^2$  (Buccheri et al. 1983), *PowSpec*/Xronos<sup>4</sup> v5.21, and *Scargle*/Midas (Scargle 1982) periodograms. All methods were applied on background-subtracted light curves, with times corrected to the solar barycentric system. The  $Z_n^2$  and *PowSpec* were also applied directly on the *pn* event lists. We adopt the 0.6–2 keV, 2–12 keV, and 0.6–12 keV energy bands in all cases. The timing resolution of 200 ms is set by the *pn* *extended full window* mode, corresponding to a Nyquist frequency of 2.5 Hz.

Applied to the 0.6–12 keV event lists, the  $Z_n^2$  tool fails to detect any significant coherent signal in the frequency range 0.005–2.5 Hz. The upper limit on the pulsed fraction is  $\sim 2.5\%$ . We searched for low frequency signals using the *Scargle* power spectrum applied on the 0.6–12 keV light curves binned at 150 s. Although quasi-periodic variability exists during each epoch on time scales of 300 s up to several ks, Figure 7 (top) shows that no peak is common to all XMM-*Newton* observations. In particular, we do not find any power at the 14 ks period found by Torrejón & Orr (2001) in the BeppoSAX data.

As visible on Figure 4, the hardness ratio exhibits long period oscillations with a pattern of variability apparently uncorrelated with that of the total flux. Interestingly, the *Scargle* hardness ratio power spectra of OBS. 1 and 3 both show peaks at the BeppoSAX period of 14 ks. Such a peak is absent in OBS. 2, in which a new feature appears at about 9 ks (Fig. 7, bottom). Finally, a peak at  $P \sim 37$  ks is common to all observations. However, because this is the order of the observing windows of the three observations, it is doubtful that such an oscillation is real.

Figure 8 shows the *Scargle* power spectrum of the three observations merged in a single time series. The 0.6–12 keV flux does not exhibit strong coherent low frequency signal. In contrast the hardness ratio power spectrum displays marked artifacts at  $P \sim 37$  ks, and a possible real feature at  $\sim 14$  ks.

To check for recurrences in the emission of HD 110432, we have also calculated the autocorrelation function from light curves and their inversed fluxes – in order to emphasize the times of low flux (see Fig. 9), using the *Autocor*/Xronos v5.21. No pattern is evident.

<sup>4</sup> <http://heasarc.nasa.gov/docs/xanadu/xronos/xronos.html>

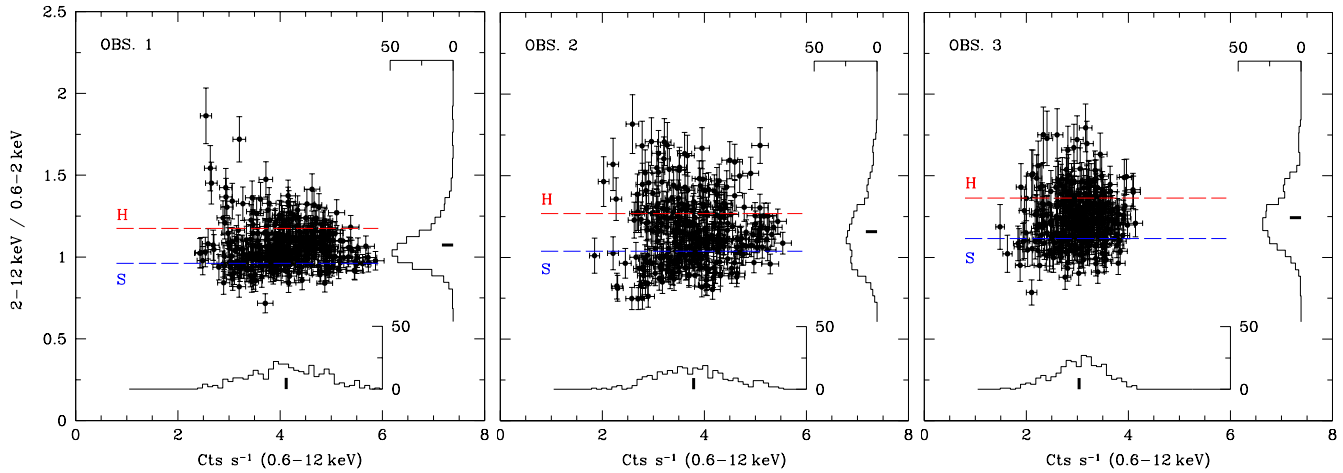


**Fig. 5.** Hardness-intensity X-ray diagrams. The insets show the intensities and hardness distributions, in which their mean values are marked. The data are grouped in time bins of 150 s. The horizontal lines indicate the limit of the adopted hard and soft states.

**Table 6.** Best-fit parameters of the X-ray spectra derived in soft (S) and hard (H) states, obtained from a M1-like model.

	OBS. 1		OBS. 2		OBS. 3	
	S	H	S	H	S	H
$N_H (10^{22} \text{ cm}^{-2})$	$0.28_{-0.02}^{+0.03}$	$0.48_{-0.07}^{+0.08}$	$0.30_{-0.03}^{+0.02}$	$0.69_{-0.12}^{+0.12}$	$0.40_{-0.04}^{+0.04}$	$0.57_{-0.06}^{+0.07}$
$kT_1 (\text{keV})$	$0.84_{-0.22}^{+0.46}$	$0.55_{-0.17}^{+0.11}$	$0.65_{-0.12}^{+0.15}$	$0.50_{-0.27}^{+0.12}$	$0.59_{-0.12}^{+0.17}$	$0.65_{-0.19}^{+0.23}$
$f_{T_1} (\text{erg cm}^{-2} \text{s}^{-1})$	$6.6 \times 10^{-13}$	$2.2 \times 10^{-12}$	$7.2 \times 10^{-13}$	$5.3 \times 10^{-12}$	$9.5 \times 10^{-13}$	$1.1 \times 10^{-12}$
$kT_2 (\text{keV})$	$5.67_{-2.98}^{+74.22}$	$5.56_{-1.64}^{+3.17}$	$3.18_{-1.02}^{+1.24}$	$3.20_{-1.49}^{+4.38}$	$3.6_{-1.00}^{+1.80}$	$7.04_{-1.81}^{+1.99}$
$f_{T_2} (\text{erg cm}^{-2} \text{s}^{-1})$	$5.9 \times 10^{-12}$	$1.2 \times 10^{-11}$	$3.8 \times 10^{-12}$	$5.9 \times 10^{-12}$	$6.0 \times 10^{-12}$	$1.3 \times 10^{-11}$
$kT_3 (\text{keV})$	$13.40_{-9.55}^{+4.55}$	$26.15_{-10.93}^{+21.86}$	$20.62_{-5.47}^{+10.10}$	$23.50_{-7.60}^{+8.54}$	$28.13_{-8.35}^{+20.64}$	$> 54.67$
$f_{T_3} (\text{erg cm}^{-2} \text{s}^{-1})$	$3.6 \times 10^{-11}$	$3.7 \times 10^{-11}$	$2.7 \times 10^{-11}$	$3.8 \times 10^{-11}$	$3.1 \times 10^{-11}$	$3.2 \times 10^{-11}$
$\chi^2/\text{d.o.f}$	0.97/87	1.01/77	1.10/97	0.99/71	1.01/95	1.08/90

Notes:  $f_{T_i}$  is the unabsorbed 0.2–12 keV flux of the  $kT_i$  component. The abundances, and the central energy and dispersion of the Gaussian lines are those of M1 in Table 2. Quoted errors are at the 90% confidence level.

### 6.3. Power density spectrum

We plot in Fig. 10 the power spectra computed by *PowSpec/Xronos* v5.21 on the 0.6–12 keV *pn* events, accumulated in time bins of 5 s. The power steadily rises at low frequencies, similar to what is observed in  $\gamma$  Cas (Smith et al. 1998a; Robinson & Smith 2000). At frequencies below  $\sim 0.003$  Hz, the spectra have the usual *power law* shape with an index of  $\sim 0.72$ – $0.84$  up to a break at  $f \sim 0.01$  Hz, where the white noise dominates. The *power law* index is significantly smaller than one – and mutually consistent for all observations at  $1\sigma$  (see values in Fig. 10, computed from  $10^{-4}$  to  $5 \times 10^{-3}$  Hz) –, indicating that the low frequency behaviour of HD 110432 might be somewhat different from that of  $\gamma$  Cas. The difference could lie either in the frequency of intermediate-timescale (< few hour) flux “undulations” or in the relative numbers of strong and weak flares.

## 7. Discussion

### 7.1. HD 110432: a $\gamma$ Cas analog system

HD 110432 has X-ray and optical properties that are similar to those observed in  $\gamma$  Cas. Contrary to “normal” O-B stars which are usually soft ( $kT \sim 0.5$  keV; Berghöfer et al. 1996) and modest ( $L_X \sim 10^{31}$ – $32$  erg s $^{-1}$ ; Berghöfer et al. 1997) X-ray sources, HD 110432 and  $\gamma$  Cas emit preferentially hard X-rays at moderate luminosities. In addition to the classical soft emission normally observed in B stars, a warm ( $\sim 1$ – $5$  keV) component is needed to fit an otherwise dominant hard continuum in  $\gamma$  Cas ( $kT \sim 12$  keV; White et al. 1982; Murakami et al. 1986; Parmar et al. 1993; Horaguchi et al. 1994; Smith et al. 1998a; Kubo et al. 1998; Owens et al. 1999; Smith et al. 2004). Iron K lines (Fe XXV and Fe XXVI) as well as a fluorescent component at 6.4 keV are seen in emission. As for HD 110432, the light curve of  $\gamma$  Cas displays strong variability on time scales ranging from the photon limit of the instrument to several minutes, in the form of flare-like events (Murakami et al. 1986; Smith et al. 1998a; Robinson & Smith 2000). The intrinsic luminosity of the *cool* component of HD 110432

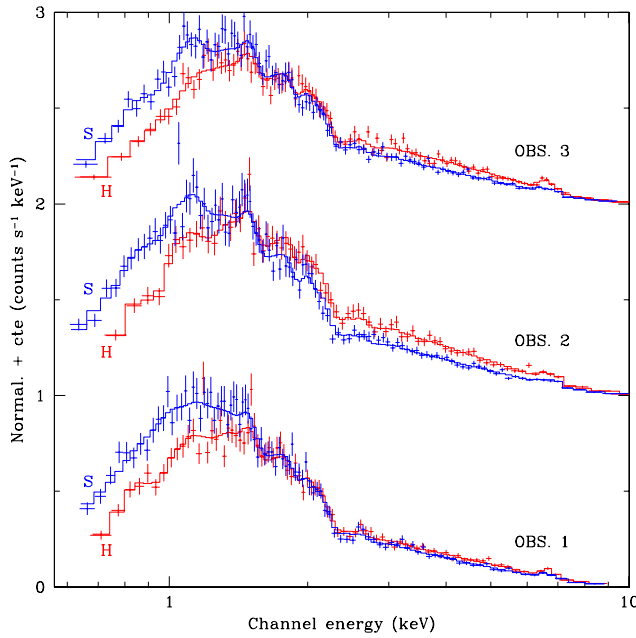


**Fig. 6.** X-ray spectra during high (H) and soft (S) states. Spectra are normalized and added to a constant term. The solid lines represent the resulting fits shown in Table 6.

$[\sim (5-10) \times 10^{30} \text{ ergs}^{-1}, \text{ in } 0.1-2.4 \text{ keV}]$  is comparable to the shocked-wind emission displayed by “normal” B stars. On the other hand, the suspected variability by a factor of  $\sim 5$  in the unabsorbed soft-energy flux is in contrast with the X-ray variability in this energy regime in “normal” B stars.

The intensity and hardness variabilities, and the multi-temperature model needed to describe the X-ray emission of HD 110432, and  $\gamma$  Cas (Smith et al. 2004), strongly suggest a complex X-ray environment. We did not find any evidence for coherent pulsations of short periodicities in HD 110432. However, there is some evidence for the presence of preferred time scales of variability, the 14 ks period, seen in both the hardness ratio in two of our observations and in the BeppoSAX light curve discussed by Torrejón & Orr (2001).

Over the last several years the claims of transitory oscillations have become almost a rule in the X-ray literature of  $\gamma$  Cas, and now perhaps of  $\gamma$  Cas analogs. The transience of these oscillations cannot in our opinion be altogether dismissed as due only to inadequately sampled data or to short observing times – although we suspect these causes will also play a role in some of them.

Consider first for  $\gamma$  Cas that Frontera et al. (1987) reported the existence of a 6 ks period in a continuous 22 ks *EXOSAT* light curve. This period could not be found by Parmar et al. (1993) in a nearly continuous 30 hour light curve subsequently obtained by the same instrument, nor has it been rediscovered in many light curves obtained since then. The same holds true of the report by Haberl (1995), on the basis of four short stretches of *Rosat* that a period of 8.1 ks might exist in the soft X-ray. However,

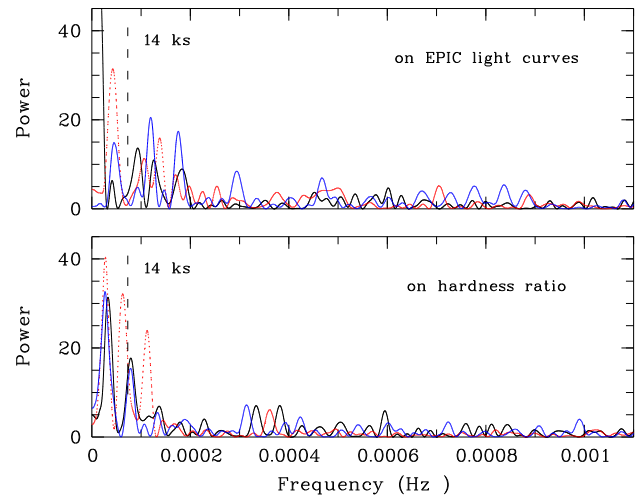


**Fig. 7.** Power spectra at low frequencies from 0.6–12 keV light curves and from  $(2-12 \text{ keV})/(0.6-2 \text{ keV})$  hardness ratio, binned to 150 s. Black: OBS. 1, red: OBS. 2, and blue: OBS. 3.

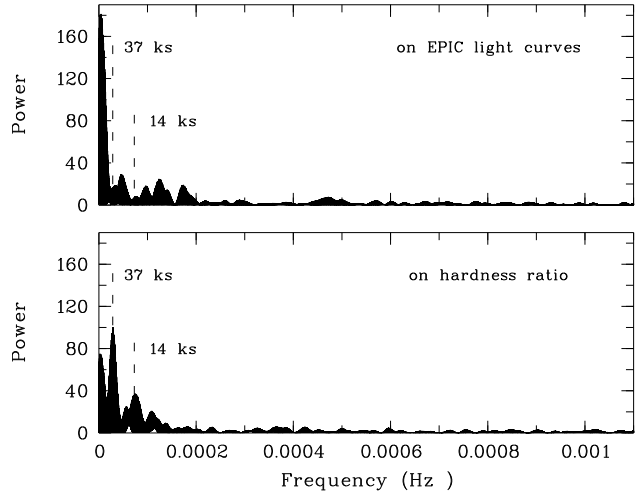


**Fig. 8.** Same as Fig. 7, but for power spectra computed on the merged 1, 2, and 3 observations.

since the termination of the *Rosat* satellite, it has been impossible to establish that this component, at 200 eV, might recur – unless it were to be associated with an oscillation of the dominant component of this star’s 12 keV emission. On the basis of a long train of *RXTE* observations of  $\gamma$  Cas, Robinson & Smith (2000) discovered a 7–7.5 hour variation in the *inverse flux* light curve. Interestingly, this oscillation was rediscovered in a recurrent flickering of the high velocity wind component of the CIV and SiIV resonance lines from a series of 1982 *IUE* observations (Cranmer et al. 2001). In a follow-up with six *RXTE* inverse flux curves, Robinson & Smith (2000) found the 7–7.5 hour oscillation in one of them and a 3.5 hour and a 5.8 hour oscillation in two more; no trace of any was found in the other three. Thus, both in  $\gamma$  Cas and in HD 110432 a dominant transient oscillation seems to be sometimes present,

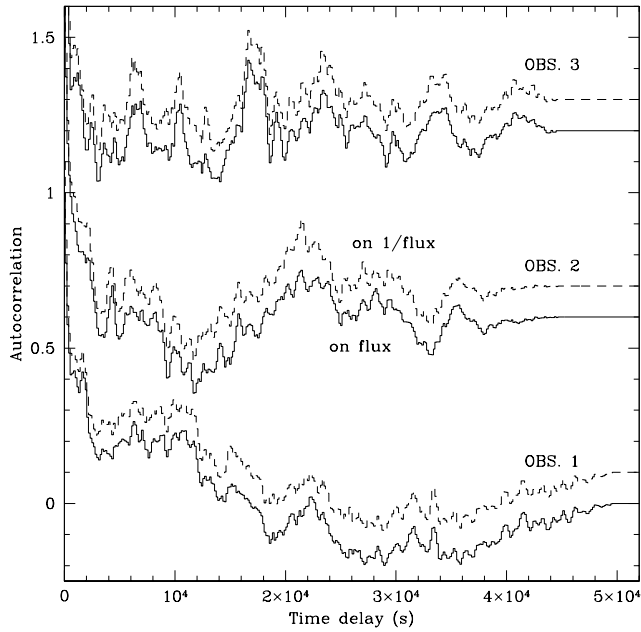


**Fig. 9.** Autocorrelation from 0.6-12 keV light curves (solid lines) and from their inversed fluxes, added to constant terms.

other times absent, and occasionally accompanied by a second one.

Recently, Lopes de Oliveira et al. (2006) have documented a 3.2 ks oscillation in a long X-ray flux curve of HD 161103. However, after 3–4 cycles, the oscillation eventually damped out in all energies. We also note a report by Safi-Harb et al. (2006) of a weak 1.5 ks period in *Chandra* and *XMM-Newton* light curves of HD 119682, which these authors have advanced as the newest  $\gamma$  Cas candidate analog. However, no information is available on the statistical robustness of these temporal variations.

What is one to make of these peculiar oscillations? The accumulating evidence suggests that they represent true detections of noncoherent oscillations. We cannot state at this time what might give rise to these oscillations, which perhaps might be best described as relaxation cycles. However, if we accept that they are not strictly repeating, it becomes easier to state what they cannot be. The fact that oscillations can damp out and that they can also accompany other oscillations in the same data sequence (e.g. Fig. 7) suggests that they cannot be explained by a rotational or orbital stellar (or disk) modulation. For now we are free to speculate only that the transience of these oscillations are a fundamental attribute of the X-ray generation mechanism.

We have noted that HD 110432 and  $\gamma$  Cas also display striking similarities in their optical spectra. The emission features in the yellow-red spectra confirm the information from the Balmer line emissions that the Be disks are extensive and probably dense. They also provide information on the thermodynamic description and the viewing aspect of the disk. The appearance of migrating subfeatures in the line profiles is similar to their appearance

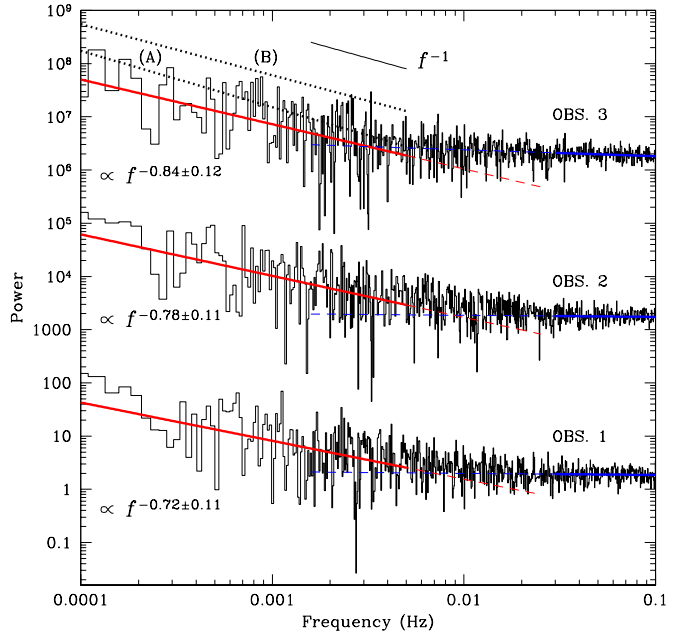


**Fig. 10.** Power spectra from 0.6-12 keV *pn* data binned to 5s. For clarity, results of the second and third observations were multiplied by factors of  $10^3$ . A  $f^{-1}$  profile is shown for comparison. The dotted lines (both offset by convenience) represent the  $f^{-1.06 \pm 0.05}$  (A) and the  $f^{-0.96 \pm 0.04}$  (B) profile derived from the  $\gamma$  Cas's *RXTE* data on March 1996 and November 1998 (after Robinson & Smith 2000), respectively.

in the UV and optical spectrum of  $\gamma$  Cas. In the latter case one can also state that this is consistent with the brief appearances of UV continuum absorptions that seem to be formed by transiting clouds forced into corotation around the Be star (Smith et al. 1998b) by a putative magnetic field and which are arguably anticorrelated with X-ray variations having several hour timescales (Smith et al. 1998a). As noted above, the 130 day modulation of the 2002 optical light may well be an analog of the now well-documented optical cycles of  $\gamma$  Cas. These in turn correlate well with  $3\times$ -amplitude X-ray cycles in  $\gamma$  Cas (Robinson et al. 2002; Smith & Balona 2006).

For both HD 110432, and  $\gamma$  Cas, the UV-derived ISM column density is only about 1/10 of that one finds from modeling the soft X-rays, and therefore the most of the column density is due to local absorptions.

Altogether, the set of X-ray and optical properties of HD 110432 confirm its classification as a member of the newly established class of  $\gamma$  Cas-like stars as proposed by Motch et al. (2006) and Lopes de Oliveira et al. (2006).

## 7.2. Spectral changes

Our spectral and timing analysis reveal the complex behaviour of the X-ray emission of HD 110432 on short ( $\sim$  tens to thousand of seconds) as well as on large time scales ( $\sim$  months–year).

Strong and rapid variabilities are clearly observed in soft and hard light curves, even though apparently non-coherent, in time scales as short as  $\sim 10$  s. Such shots, exhibiting increases up to  $\sim 100\%$  in flux, are superimposed over a long-term ( $\sim 5$ – $10$  ks) trends of the X-ray emission, but their occurrence and intensity do not depend upon whether the source is in a “low” or “high” state. This chaotic behaviour strongly suggests the existence of numerous non-cospatial X-ray active regions, resulting in shots through flare-like events. In this picture, the basal component would be due to an averaged emission of a collection of a large number of such active regions. Actually, the best fitting 3-T models show that several distinct emitting regions of different temperatures, emission measures and fluxes, and probably column densities contribute to the overall X-ray energy distribution on large time scales. The variability of these parameters in different putative sites seems so far uncorrelated.

The X-ray emission of HD 110432 is dominated by a *hot*-thermal component, which accounts for  $\sim 80\%$  of the unabsorbed 0.2–12 keV flux. Its *warm* and *cool* components represent the other  $\sim 18\%$  and  $\sim 2\%$ . The unabsorbed X-ray flux of HD 110432 has steadily decreased over the two first XMM-*Newton* observations, increasing during the last observation. This trend was apparently accompanied by a slight hardening of the X-ray spectrum.

The EM of the *hot* component seems to decrease by  $\sim 10\%$  over the subsequent observations, while the EM of the *cool* and *warm* components follow a more complicated pattern, which is anti-correlated one with another. If the different plasmas have similar densities, our results show that the total emitting volume in all observations is dominated by the *hot* component ( $\sim 70$ – $80\%$ ), with a small contribution of the *warm* ( $\sim 15$ – $25\%$ ) and *cool* (few percents) components.

The EPIC energy band (0.2–12 keV) does not extend enough in the hard X-rays to really constrain the high temperatures ( $\gtrsim 20$  keV) derived for the hot emission of HD 110432. The fits logically give large errors, and the temperatures in each epochs are in the limits of the 90% confidence level. However, the varying relative intensity of the ionized iron lines (Fig. 3) suggest that the physical parameters of the X-ray environment has changed in different epochs.

### 7.3. Origin of the X-ray emission

In spite of several X-ray campaigns of  $\gamma$  Cas, the true nature of its X-ray emission remains an open question: accretion onto a degenerate companion or magnetic active Be star? This controversy itself extends to HD 110432 and all  $\gamma$  Cas-analog systems.

#### 7.3.1. Be/X-ray binary?

Accretion onto a degenerated companion star has been invoked to explain the anomalous, variable X-ray flux of

$\gamma$  Cas, mainly due its moderate luminosity – of about  $10^{32}$ – $33$  erg s $^{-1}$  in 0.2–12 keV. This could be easily obtained if matter is falling directly onto a NS either from the Be star’s wind or its decretion disk ( $\dot{M}_{acc} \sim 3 \times 10^{-13} M_{\odot}$  yr $^{-1}$ ), or conceivably (though not easily) a WD ( $\dot{M}_{acc} \sim 3 \times 10^{-10} M_{\odot}$  yr $^{-1}$ ) – and hard emission. Following the hard-thermal nature of its X-rays, typical of CVs and in contrast with the non-thermal emission detected in all well-known classic Be+NS systems, and despite the lower yield in luminosity, a WD is preferred instead of a NS.

Be+WD systems are predicted by several massive binary evolution models to be the outcomes describing the evolution of massive binary systems. This configuration is expected for all B types, with a distribution peaking around the B2–3 types (Pols et al. 1991). Typical models predict that these systems should comprise about 70% of the total evolved Be binary outcomes (van den Heuvel & Rappaport 1987; Waters et al. 1989; Pols et al. 1991; van Bever & Vanbeveren 1997; Raguzova 2001). However, we note that this fraction depends sensitively on the final mass of the B primary such that it is low for evolved systems with early B primaries. Thus, in these computations all known Be/X-ray binaries have a companion NS (see Raguzova & Popov 2005, for a recent compilation of Be/X-ray properties). So far no Be+WD system has been identified. On the basis of their X-ray properties, notably their (i) hard-thermal spectra, (ii) iron lines, (iii) luminosities, and (iv) variability, that are reminiscent of similar properties in some CVs, the  $\gamma$  Cas analogs are tenable Be+WD candidates. However, one difference we can point out is that, as discussed below, the analogs seem to show a low Fe abundance according to the FeK line strengths – this is not generally true for Fe abundances derived in WD systems. Another possible example of a Be+WD system might be the super-soft X-ray source XMMU J052016.0–692505, associated to a B0-3e star in the LMC, as proposed by Kahabka et al. (2006). Its black-body emission, with bolometric luminosity  $\gtrsim 10^{34}$  erg s $^{-1}$ , was interpreted as probably being due to a stable nuclear burning WD, accreting from the Be star’s decretion disk.

In CV systems a WD primary, strongly magnetized or not, accretes from a Roche lobe-filling, late-type evolving secondary star. An accretion disk is commonly formed in non-magnetic systems. However, it tends to be inhibited by the magnetic field lines in strongly magnetized ( $\sim 10^{10}$  G) stars. In both types of systems accretion shocks onto the WD or the boundary layer between the WD’s surface and a putative disk will result in a X-ray spectrum characterized by plasma temperatures ranging from a few keV to tens of keV. Their luminosities are moderately high ( $\sim 10^{32}$ – $33$  erg s $^{-1}$ ). Interestingly, the X-rays are typically modeled as emissions of plasmas having at least a few components and indeed perhaps a broad continuous temperature distribution. The latter possibility is typical of a cooling process, e.g. in which the emission measure of each temperature component scales with the temperature as  $dEM/dT \propto T^{\alpha}$ .

The prominent ionized iron lines, FeXXVI and FeXXVI, and the fluorescent 6.4 keV iron feature, present in HD 110432 and in all  $\gamma$  Cas analogs so far are also reminiscent of those detected in several CV systems, with similar EWs and intensities (Hellier et al. 1998; Ezuka & Ishida 1999). Curiously, Ezuka & Ishida (1999) noted that the ionization temperature derived from FeK lines in CVs are systematically lower than that derived from continuum, as we found for HD 110432 (Section 5.3).

In fact,  $\gamma$  Cas, the prototype of this class, itself is a component of a binary system. The orbit of this system has a  $P_{\text{orb}} \sim 204$  days with an eccentricity of 0.26 (Harmanec et al. 2000) or in a near-circular orbit (Miroshnichenko et al. 2002). The secondary mass is roughly  $1 M_{\odot}$ , but its nature is otherwise unknown. We rule out the accreting NS picture because of the thermal nature of the observed X-rays. We also point out that according to binary evolution theory there appear to be difficulties in producing a B0.5e+WD system as a typical outcome.  $\gamma$  Cas's mass of  $\sim 15\text{--}18 M_{\odot}$  (Stee et al. 1995; Harmanec et al. 2000) appears to be near the limit where a WD secondary can be produced. On the other hand, our current knowledge on binary evolution requiring material exchange between stars is such that we cannot conclusively rule out a  $\gamma$  Cas+WD system. In any case, this is not a decisive argument against the presence of a white dwarf companion for HD 110432, for which Zorec et al. (2005) have derived a mass of only  $9.6 M_{\odot}$ . The binary status of HD 110432 and all other  $\gamma$  Cas-analog candidates is unknown. If HD 110432 actually belongs to the  $\sim 60$  Myr old open cluster NGC 4609 (Feinstein & Marraco 1971), then the largest age for a  $9.6 M_{\odot}$  B1IVe star of  $\sim 20$  Myr would suggest that HD 110432 is a blue straggler. Interestingly, two other GCas candidates, the star in NGC 6649 (Marco et al. 2006) and HD 119682 (Safi-Harb et al. 2006) also appear to be blue stragglers. Therefore, an evolved status may be a prerequisite to the source being a peculiar X-ray emitter. An advanced age could hint at a few scenarios for the X-ray production, such an accreting binary companion, or a Be star with a strong surface field resulting from the buoyant rise of flux through the star's radiative interior (e.g. MacGregor & Cassinelli 2003).

It is also not yet clear that a WD in a Be binary system as widely spaced as  $\gamma$  Cas could accrete enough material from the wind to account for the observed X-ray luminosity. In particular, the tidal torquing of the Be disk by the secondary star may effectively truncate the disk inside the secondary's orbital radius (Okazaki & Negueruela 2001), which would result in too little mass accretion to be important. Interestingly, there is no detected correlation between X-ray flux and the orbital phase of  $\gamma$  Cas (RXTE observations; Robinson et al. 2002), or outburst. This could be explained if the accreting star were in a nearly circular orbit close to the plane of the Be decretion disk.

For completeness, we point out that the  $\gamma$  Cas-like systems HD 161103 and HD 119682 exhibit 3.2 ks (XMM-Newton; Lopes de Oliveira et al. 2006) and 1.5 ks (XMM-

Newton and Chandra; Safi-Harb et al. 2006) oscillations, respectively. If these should turn out to be stable, they could be the signature of a spinning compact object.

### 7.3.2. Magnetic active Be star?

Evidence is accumulating in favor of magnetic activities in  $\gamma$  Cas and HD 110432, that could produce the X-ray emission in these objects. The fundamental question of whether these stars are magnetic seems less hypothetical with the discovery of a coherent variation over 9 years with a photometric period of 1.21 days in the optical  $B, V$  passbands (Smith & Balona 2006). This periodicity appears to be best explained by a feature on the star's surface, since 1.2 days is consistent with the star's expected radius, rotational velocity, and obliquity. Perhaps also relevant are the recurrent blue-to-red "migrating substructures" (*msf*) seen in the line optical profiles of both stars often (Yang et al. 1988; Smith & Robinson 1999; Smith & Balona 2006). These features are reminiscent of the active and rapidly rotating pre-main sequence K star AB Dor (Collier Cameron & Robinson 1989). The *msf* are most easily interpreted as being due to corotating clouds anchored onto the stellar surface by magnetic confinement (Smith et al. 1998b). In addition, the  $\sim 3\text{--}4\%$  sinusoidal modulations in the  $B$  and  $V$  photometric bands with a timescales of 130 days detected in HD 110432 (Smith & Balona 2006) are reminiscent of the optical cycles reported in  $\gamma$  Cas, which are best explained by variations in the integrated flux of the Be disk (Smith et al. 1998b, 2006).

The key assumption of the scenario in which X-rays are due to magnetic activity is that the Be star has a surface magnetic field some fraction of which threads into the inner regions of its ionized circumstellar disk (Robinson et al. 2002, and references therein). According to the hypothesis of RSH02, field entrainment produces turbulence within the disk and the difference in angular velocities between the disk and the star stresses and shears magnetic lines. Magnetic reconnection leads to the ejection of high energy particles which impact the Be star and generate hard X-ray emission. This scenario is supported by UV observation of highly redshifted line absorptions in HD 110432 that could be manifestations of accelerated material (Smith & Robinson 1999). In this context,  $\gamma$  Cas analogs may be related to magnetic Op and Bp stars like  $\theta^1$  Ori C (Donati et al. 2002). As part of a star-disc interaction, X-rays could be modulated by a dynamo-like process within the Be's circumstellar disk (Robinson et al. 2002), accounting for the almost unabsorbed soft X-ray emission. A dense circumstellar disk in  $\gamma$  Cas analogs seems to be a needed ingredient for the magnetic picture.

It is not yet clear how observations might eventually provide quantitative constraints on the star-disc magnetic picture. Similarly, the theory is not yet developed enough to predict a characteristic temperature or to explain the presence of plasma with more than one temperature. According to the X-ray variabilities detected in

$\gamma$  Cas analogs, the surface of these stars would have to have a complicated magnetic topology. In any case, the  $1/f$  tendency roughly observed in the periodogram at low frequencies is in agreement with stochastically appearing blobs. Indeed, at this point dynamo models also cannot make sensible predictions for *any* astrophysical environment (including the solar interior). In addition, there are questions as to how the putative disk dynamo can acquire an organized cyclical variability, as opposed to the more common situation where the dynamo is chaotic, and whether the disk dynamo can survive the intrusion of too much of the stellar field (Smith et al. 2006).

## 8. Conclusions

HD 110432 is a member of the recently discovered class of  $\gamma$  Cas-analogs (Motch et al. 2006; Lopes de Oliveira et al. 2006), according to its X-ray and optical properties, summarized as follows. This class is composed of Be stars having X-ray properties described by moderately luminous and variable light curves ( $\sim 10^{32-33} \text{ erg s}^{-1}$ ; 0.2–12 keV) and spectra indicative of multiple thermal components dominated by a hard component ( $kT \gtrsim 7 \text{ keV}$ ; current limit determined by HD 161103; Lopes de Oliveira et al. 2006). No outbursts are observed up to now. The thermal origin of their X-ray emissions is strongly supported by the presence of a Fe K $\alpha$  complex. Curiously, all identified members are B0.5–B1 stars with very large and nearly symmetrical H $\alpha$  profile, and FeII emission lines, supporting dense and/or large and likely stable circumstellar disks. *In toto*, these features are not exhibited in optical and X-ray spectra and light curves of “normal” Be stars or known Be/X-ray binaries.

The X-ray spectrum of HD 110432 is very complex and variable. It results from a composition of three thermal plasmas but is dominated by a hard component of  $kT \sim 21\text{--}39 \text{ keV}$  that accounts for about  $\sim 80\%$  of the total flux. HD 110432 is, thus, the hottest known Be star in the X-ray waveband. In addition to the iron lines detected in  $\gamma$  Cas-analogs, a variable Fe XXVI Ly $\beta$  (8.2 keV) in emission is detected for HD 110432, in agreement with its hot and variable X-ray component. Notably, its light curve exhibits rapid and strong variations, in soft and hard X-ray bands throughout the 0.2–12 keV range. These variations are followed by long term variations and flare-like events in the source’s hardness recurrent in few tens of seconds. There is no evidence for high-frequency pulsations, but the low-frequency analysis reveals unstable long-term variations in timescale of  $\sim 3\text{--}4$  hours.

Although our X-ray spectral analysis is consistent with the presence of an accreting white dwarf for HD110432, we cannot exclude for this star star the magnetic star-disk interaction scenario, proposed for  $\gamma$  Cas by Robinson et al. (2002) and references. The presence or absence of binarity of HD 110432, and if appropriate, the description of its orbit, will provide the means to make substantial progress in elucidating the processes behind its X-ray emission.

*Acknowledgements.* R.L.O. acknowledges financial support from Brazilian agencies FAPESP (grant 03/06861-6) and CAPES (grant BEX0784/04-4), and the Observatoire de Strasbourg (CNRS). I.N. is a researcher of the programme *Ramón y Cajal*, funded by the Spanish Ministerio de Ciencia y Tecnología (currently Ministerio de Educación y Ciencia) and the University of Alicante, with partial support from the Generalitat Valenciana and the European Regional Development Fund (ERDF/FEDER). This research is partially supported by the MCyT (currently MEC) under grant AYA2005-00095.

## References

Ballereau, D., Chauville, J., & Zorec, J. 1995, A&AS, 111, 423

Barrera, L. H., Mennickent, R. E., & Vogt, N. 1991, AAS, 185, 79

Berghöfer, T.W., Schmitt, J.H.M.M., & Cassinelli, J.P. 1996, A&AS, 118, 481

Berghöfer, T.W., Schmitt, J.H.M.M., Danner, R., & Cassinelli, J.P. 1997, A&A, 322, 167

Bohlin, R. C. 1970, ApJ, 162, 571

Buccheri, R., Bennett, K., Bignami, G.F., et al. 1983, A&A, 128, 245

Codina, S.J., de Freitas Pacheco, J.A., Lopes, D.F., & Gilra, D. 1984, A&AS, 57, 239

Collier Cameron, A., & Robinson, R. D. 1989, MNRAS, 236, 57

Cranmer, S. R., Smith, M.A., & Robinson, R. D. 2000, ApJ, 533, 433

Donati, J.-F., Babel, J., Harries, T. J., Howarth, I. D., Petit, P., & Semel, M. 2002, MNRAS, 333, 55

Draper P.W., Taylor, M., & Allan 2000, Starlink Users Note 139.12, R.A.L.

Ezuka, H., & Ishida, M. 1999, ApJSS, 120, 277

Feinstein, A., & Marraco, H. G. 1971, PASP, 83, 218

Frémat, Y., Zorec, J., Hubert, A.-M., & Floquet, M. 2005, A&A, 440, 305

Frontera, F., Dal Fiumi D., Robba, N. R., et al. 1987, ApJ, 320, L127

Haberl, F. 1995, A&A, 296, 685

Harmanec, P., Habuda, P., Stefl, S., et al. 2000, A&A, 364, L85

Hellier, C., Mukai, K., & Osborne, J.P. 1998, MNRAS, 297, 526

Horaguchi, T., Kogure, T., Hirata, R., et al. 1994, PASJ, 46, 9

Kahabka, P., Haberl, F., Payne, J. L., & Filipović, M. D. 2006, A&A, 458, 285

Kharchenko, N.V., Piskunov, A.E., Röser, S., Schilbach, E., & Scholz, R.-D. 2005, A&A, 438, 1163

Kilkenny, D., Whittet, D.C.B., Davies, J.K., et al. 1985, SAAOC, 9, 55

Kubo, S., Murakami, T., Ishida, M., & Corbet, R.H.D. 1998, PASJ, 50, 417

Lopes de Oliveira, R., Motch, C., Haberl, F., Negueruela, I., & Janot-Pacheco, E. 2006, A&A, 454, 265

MacGregor, K.B., & Cassinelli, J.P. 2003, ApJ, 586, 480

Marco, A., Negueruela, I., & Motch, C. 2006, in Moffat, A.F.J., & St.-Louis, N. (eds.), *Proceedings of Massive Stars in Interacting Binaries*, Hotel Sacacomie, Montreal, Quebec, Canada, August 2004, ASP Conference Series, in press

Miroshnichenko, A.S., Bjorkman, K.S., & Krugov, V.D. 2002, *PASP*, 114, 1226

Motch, C., Haberl, F., Dennerl, K., Pakull, M., & Janot-Pacheco, E. 1997, *A&A*, 323, 853

Motch, C., Lopes de Oliveira, R., Negueruela, I., Haberl, I., & Janot-Pacheco 2006, in *Active OB Stars: Laboratories for Stellar & Circumstellar Physics*, ed. S. Stefl, S. P. Owocki, & A. Okazaki, ASP Conf. Ser., in press [ASTRO-PH 0512556]

Murakami, T., Koyama, K., Inoue, H., & Agrawal, P. C. 1986, *ApJ*, 310, 31

Okazaki, A.T. 1991, *PASJ*, 43, 75

Okazaki, A.T., & Negueruela, I. 2001, *A&A*, 377, 161

Owens, A., Oosterbroek, T., Parmar, A.N. et al. 1999, *A&A*, 348, 170

Perryman, M.A.C. 1997, *The Hipparcos and Tycho Catalogues*, ESA SP-1200 (Noordwijk: ESA)

Parmar, A.N., Israel, G.I., Stella, L., & White, N. E. 1993, *A&A*, 275, 227

Pols, O.R., Coté, J., Waters, L.B.F.M., & Heise, J. 1991, *A&A*, 241, 419

Rachford, B.L., Snow, T.P., Tumlinson, J., et al. 2001, *ApJ*, 555, 839

Raguzova, N.V. 2001, *A&A*, 367, 848

Raguzova, N.V., & Popov, S.B. 2005, ASTRO-PH 0505275

Rakowski, C.E., Schulz, N.S., Wolk, S. J., & Testa, P. 2006, *ApJ*, 649, L111

Robinson, R.D., & Smith, M.A. 2000, *ApJ*, 540, 474

Robinson, R.D., Smith, M.A., & Henry, G. W. 2002, *ApJ*, 575, 435

Safi-Harb, S., Ribo, M., Butt, et al. 2006, submitted to *ApJ* [ASTRO-PH 0607551]

Scargle, J.D. 1982, *ApJ*, 263, 835

Shortridge K., Meyerdicks H., Currie, M. et al. 1997, *Starlink User Note* 86, 15, R.A.L.

Slettebak, A. 1982, *ApJS*, 50, 55

Slettebak, A., Collins, G.W., & Truax, R. 1992, *ApJS*, 81, 335

Smith, M.A. 1995, *ApJ*, 442, 812

Smith, M.A., Robinson, R.D., & Corbet, R.H.D. 1998a, *ApJ*, 503, 877

Smith, M.A., Robinson, R.D., & Hatzes, A. P. 1998b, *ApJ*, 507, 945

Smith, M.A., & Robinson, R.D. 1999, *ApJ*, 517, 866

Smith, R.K., Brickhouse, N.S., Liedahl, D.A., & Raymond, J.C. 2001, *ApJ*, 556, L91

Smith, M.A., Cohen, D.H., Gu, M.F., et al. 2004, *ApJ*, 600, 972

Smith, M.A., & Balona, L. 2006, *ApJ*, 640, 491

Smith, M.A., Henry, G.W., & Vishniac, E. 2006, *ApJ*, 647, 1375

Stee, P., de Araújo, F. X., Vakili, F., et al. 1995, *A&A*, 300, 219

Torrejón, J.M., & Orr, A. 2001, *A&A*, 377, 148

Tuohy, I.R., Buckley, D.A.H., Remillard, R.A., et al. 1988, in *Physics of Neutron Stars & Black Holes* (Universal Academy Press, Tokyo), 93

van Bever, J., & Vanbeveren, D. 1997, *A&A*, 322, 116

van den Heuvel, E.P.J., & Rappaport, S.A. 1987, in *Physics of Be Stars*, IAU Coll. 92, Ed. A. Slettebak & T. P. Snow (Cambridge University Press), 291

Waters, L.B.F.M., Pols, O.R., Hogeweegen, S.J., Coté, J., & van den Heuvel, E.P.J. 1989, *A&A*, 220, L1

White, N.E., Swank, J.H., Holt, S.S., & Parmar, A.N. 1982, *ApJ*, 263, 277

Yang, S., Ninkov, Z., & Walker, G.A. 1988, *PASP*, 100, 233

Zorec, J., Frémat, Y., & Cidale, L. 2005, *A&A*, 441, 235